The Astrophysical Journal, 778:37 (9pp), 2013 November 20 doi:10.1088/0004-637X/778/1/37

HIGHLY CONCENTRATED NEBULAR NOBLE GASES IN POROUS NANOCARBON SEPARATES FROM THE SARATOV (L4) METEORITE

Sachiko Amari[1], Jun-ichi Matsuda[2], Rhonda M. Stroud[3], and Matthew F. Chisholm[4]
[1] McDonnell Center for the Space Sciences and the Physics Department, Washington University, St. Louis, MO 63130, USA; sa@wuphys.wustl.edu
[2] Department of Earth and Space Science, Osaka University, Osaka 560–0043, Japan
[3] Code 6360, Naval Research Laboratory, Washington, DC 20375, USA
[4] Materials Science and Technology Division, Oak Ridge National Laboratory, Oak Ridge, TN 37831, USA
Received 2013 March 29; accepted 2013 September 19; published 2013 October 31

ABSTRACT

The majority of heavy noble gases (Ar, Kr, and Xe) in primitive meteorites are stored in a poorly understood phase called Q. Although Q is thought to be carbonaceous, the full identity of the phase has remained elusive for almost four decades. In order to better characterize phase Q and, in turn, the early solar nebula, we separated carbon-rich fractions from the Saratov (L4) meteorite. We chose this meteorite because Q is most resistant in thermal alteration among carbonaceous noble gas carriers in meteorites and we hoped that, in this highly metamorphosed meteorite, Q would be present but not diamond: these two phases are very difficult to separate from each other. One of the fractions, AJ, has the highest ^{132}Xe concentration of 2.1×10^{-6} cm^3 STP g^{-1}, exceeding any Q-rich fractions that have yet been analyzed. Transmission electron microscopy studies of the fraction AJ and a less Q-rich fraction AI indicate that they both are primarily porous carbon that consists of domains with short-range graphene orders, with variable packing in three dimensions, but no long-range graphitic order. The relative abundance of Xe and C atoms ($6{:}10^9$) in the separates indicates that individual noble gas atoms are associated with only a minor component of the porous carbon, possibly one or more specific arrangements of the nanoparticulate graphene.

Key word: meteorites, meteors, meteoroids

1. INTRODUCTION

It is known that the majority of heavy noble gases (Ar, Kr, and Xe) in primitive meteorites are contained in less than 0.04% of the meteorite mass, a residue remaining after silicates are removed with HF–HCl (Lewis et al. 1975). Lewis et al. (1975) called the phase that carries the noble gases Q for quintessence. Subsequent studies (e.g., Wieler et al. 1991; 1992; Huss et al. 1996; Busemann et al. 2000; Matsuda et al. 2010a) have shown that Q contains all five noble gases, heavily fractionated relative to solar composition in favor of heavy noble gases; Q is ubiquitously present in meteorites of different compositional types and of various degrees of thermal metamorphism; and the abundance of Q decreases with an increasing degree of thermal metamorphism (e.g., Huss et al. 1996; Busemann et al. 2000). Among the four major primordial noble gas carriers in meteorites, Q (Lewis et al. 1975), diamond (Lewis et al. 1987), SiC (Tang & Anders 1988), and graphite (Amari et al. 1990), Q is most resistant to thermal metamorphism followed by diamond, SiC, and graphite (Huss et al. 1996).

Q survives HF–HCl treatment, but is readily destroyed by oxidants (Lewis et al. 1975). Reynolds et al. (1978) studied noble gases in separates from carbonaceous meteorites and suggested that Q was carbonaceous matter. Ott et al. (1981) made >10 separates from Allende HF–HCl residues and analyzed their chemical compositions and noble gas contents. Their findings that Xe contents were directly correlated with C contents and that Xe was enriched in separates with density $\leqslant 2$ g cm^{-3} indicate that Q is carbonaceous matter.

Several attempts to concentrate Q from meteorites (e.g., Moniot 1980; Ott et al. 1981; Verchovsky et al. 2002) were only partially successful. This is because primitive meteorites contain not only Q but also other forms of carbonaceous matter, which are overwhelmingly abundant and are usually removed by oxidants. We cannot use oxidants to separate Q from the other carbonaceous matter because they also destroy Q. This makes it difficult, if not impossible, to chemically separate Q from other forms of carbons in meteorites. Thus the exact nature of Q has been elusive.

Deciphering the origin and trapping mechanisms of the Q gases have also been carried out. The noble gas elemental abundance of Q in favor of heavy noble gases is indicative of adsorption. Since carbonaceous material such as charcoal is known to be an efficient adsorbent, Wacker (1989) carried out adsorption experiments on carbon and demonstrated that the enrichments in heavy noble gases observed in Q could be explained by physical adsorption at 300–400K. His result was in line with the model that the noble gases were trapped in a labyrinth, proposed by Wacker et al. (1985) and Zadnik et al. (1985). The problem, however, was that the model failed to reproduce the high release temperatures (1000°C–1200°C) of the Q gases. The fractionation that is heavily favored by heavy noble gases and the high release temperatures can be also well explained by the plasma model (Matsuda & Yoshida 2001).

The ^{3}He/^{4}He ratio of He-Q is known to be $(1.41 \pm 0.01) \sim (1.59 \pm 0.04) \times 10^{-4}$ (Wieler et al. 1991; Busemann et al. 2000). This ratio is very close to the ratio of Jupiter [$(1.66 \pm 0.05) \times 10^{-4}$], determined by the Galileo probe mass spectrometer (Mahaffy et al. 1998), but is vastly different from the solar wind ratio [$(4.64 \pm 0.09) \times 10^{-4}$] determined from the *Genesis* mission (Heber et al. 2009). Jupiter's atmospheric composition indicates that it is dominantly H_2 and He, which is similar to that of the Sun (Lodders & Fegley 1998). The difference between He in Jupiter and the solar wind He is attributed to deuterium burning, D(p, γ)^{3}He. This nuclear burning took place when the protosun was contracting on the pre-main sequence, adding ^{3}He to its original composition (e.g., Clayton 1968). No such nuclear burning took place in Jupiter, thus its ^{3}He/^{4}He ratio remains the same as that of the solar nebula. The fact that He-Q has an isotopic composition that matches that of Jupiter indicates

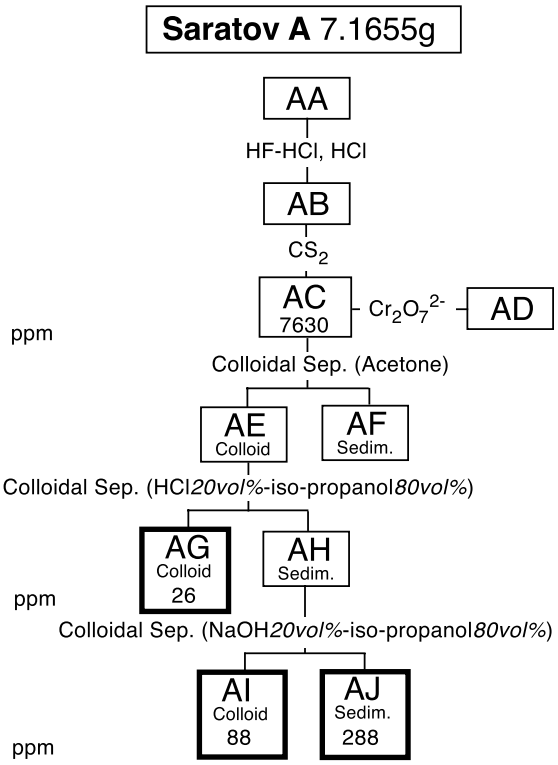

Figure 1. Separation diagram for the Saratov meteorite. The abundances are relative to the bulk meteorite. In this study, noble gas analysis was performed for AG, AI, and AJ, shown with thick lines, and TEM analysis was carried out for AI and AJ.

that Q most likely acquired its noble gases in the early solar nebula. We note, however, that Huss et al. (1996) proposed that Q gases were acquired in the molecular cloud from which our solar system formed. A better understanding of Q may therefore provide new information about the early solar system.

In the effort to better characterize Q, we report our new results obtained from the Saratov (L4) meteorite. We chose to study Saratov because Huss et al. (1996) found that the abundances of Q, diamond, and SiC decrease with increasing petrologic type (which is the indicator of thermal metamorphism), and that Q is more resistant to thermal metamorphism than the other two phases, leaving only Q in the Julesburg (L3.6) meteorite. Therefore, if Q is still present in a L4 meteorite, which experienced even higher temperatures during thermal metamorphism than Julesburg, we would be able study Q and the Q gases, especially Ne-Q, without presolar diamond, avoiding steps to separate Q and diamond. Among fairly uniform isotopic compositions of the Q gases, $^{20}Ne/^{22}Ne$ ratios of Ne-Q are an exception: the ratios can be classified into two groups (Busemann et al. 2000). Because Saratov contains Q, without the other phases that contain noble gases (Matsuda et al. 2010b), it enables us to determine a more precise $^{20}Ne/^{22}Ne$ ratio of Saratov Ne-Q.

2. EXPERIMENTAL PROCEDURE

The separation was carried out at Washington University in St. Louis (Figure 1). Starting with ~7.2 g of the Saratov meteorite, we dissolved silicates with HF–HCl and removed elemental sulfur with CS_2, yielding an HF–HCl residue AC, which consists mainly of carbonaceous matter and chromites. Noble gas data of a bulk the Saratov sample and the fraction AC, already presented by Matsuda et al. (2010b), indicated that Q is present in this meteorite. In this work, we further separated AC with three successive colloidal separations. The first colloidal separation, in which we used acetone, yielded the black colloidal fraction AE and the brown non-colloidal fraction AF at the bottom of the tube. We carried out the second colloidal separation on AE using a mixture of 20 vol.% HCl–80 vol.% isopropanol. A very small amount of the colloidal fraction AG (26 ppm relative to the bulk meteorite) was recovered. In the next step, the non-colloidal fraction AH was separated using a mixture of 20 vol.% NaOH–80 vol.% isopropanol, yielding the colloidal fraction AI (88 ppm) and the non-colloidal fraction AJ (288 ppm).

A small portion of AF and AJ were deposited on carbon planchets for the scanning electron microscopy (SEM) observation. The chemical compositions of these fractions were examined with the Noran System SIX II X-ray Microanalysis software using the JEOL JSM-840A scanning electron microscope at Washington University. We analyzed chemical compositions of ten ~5 × 5 μm areas for each fraction with a 10kV acceleration voltage. Elemental abundances in atomic percent are C = 24 ± 13, O = 48 ± 7, Mg = 0.5 ± 0.2, Al = 1.8 ± 0.4, Cr = 18 ± 4, and Fe = 8 ± 2 for AF, and C = 81 ± 7, O = 13 ± 4, Mg = 0.12 ± 0.06, Al = 0.3 ± 0.3, Cr = 4 ± 1, and Fe = 1.4 ± 0.5 for AJ. We note that since the acceleration voltage was 10kV, the Kα line of C from the carbon planchet must have been detected and added to the total C counts. Thus, the C atomic percent are overestimated, although we do not have the exact percentage of the contribution from the C planchets in the C counts. AF consists mainly of chromite ($FeCr_2O_4$) grains with a small amount of spinel ($MgAl_2O_4$) grains, while AJ consists mainly of carbonaceous matter with a lesser amount of chromite grains. Spinel grains are negligible in AJ.

The elemental abundances of all five noble gases and isotopic abundances of Ne, Ar, and Xe of fractions AG, AI, and AJ were extracted in two steps, at 600°C and 1600°C, and analyzed using the VG5400 at Osaka University, Japan. The samples were heated in a Mo crucible for 20 minutes at each temperature step to extract noble gases. After they were purified with two Ti–Zr getters at 700°C, the individual noble gases were separated from each other using a cryogenic cold trap. Residual Ar in the He and Ne fractions was removed by activated charcoal. Argon-40 was collected with a Faraday cup, while the other isotopes were analyzed with an electron multiplier in pulse-counting mode. Sensitivities and mass discrimination factors were calculated by analyzing a fixed amount of atmospheric noble gases. Uncertainties of the sensitivities, which include those of the volume of the standard air taken for analyses and statistical errors of the analyses, are about 5%. The procedural blanks at 600°C and 1600°C were analyzed before and after a series of sample measurements and were used for blank correction of individual temperature fractions. For example, the gas amounts of the procedural blank at 1600°C were ^4He = 1.3×10^{-9}, $^{22}Ne = 1.7 \times 10^{-12}$, $^{36}Ar = 3.1 \times 10^{-11}$, $^{84}Kr = 1.2 \times 10^{-12}$, and $^{132}Xe = 4.3 \times 10^{-13}$ cm^{3}STP (cm^3 at the standard temperature and pressure). In a few cases where the blank correction was more than 50%, we show the data as upper limits without the blank correction. We calculated the uncertainties of the isotopic ratios of Ne, Ar, and Xe assuming that the uncertainty of the blank amount was 100%.

The fractions AI and AJ were examined with transmission electron microscopy (TEM) at the U.S. Naval Research Laboratory (NRL) and aberration-corrected scanning transmission electron microscopy (STEM) at the Oak Ridge National Laboratory (ORNL), USA. Electron transparent samples of

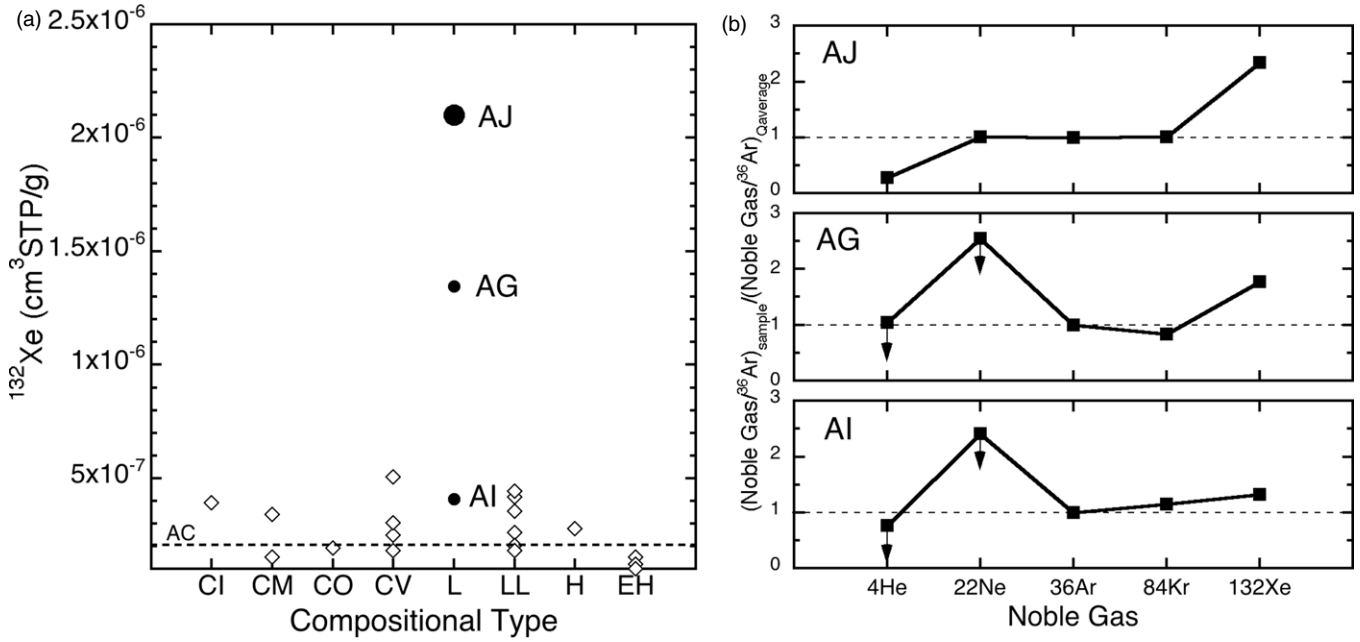

Figure 2. (a) Xe-132 concentrations of Saratov fractions AG, AI, and AJ are shown together with those of HF–HCl residues from various other types of meteorites (Huss et al. 1996; Busemann et al. 2000). The ^{132}Xe concentration of the HF–HCl residue AC (Matsuda et al. 2010b) is shown by the dotted line to illustrate how much enrichment was achieved in these Saratov fractions. (b) Noble gas abundances of AG, AI, and AJ. Noble gas concentrations were first normalized by ^{36}Ar, then to the average Q gas composition (Busemann et al. 2000). The arrows show upper limits. Xenon is more enriched in all fractions than the average, indicating a preferential enrichment of Xe.

each residue were prepared by drop casting of an aqueous suspension onto lacey carbon support films. Bright field and high-resolution TEM images, selected area electron diffraction (SAED) patterns, and energy dispersive X-ray spectra of the samples were obtained with the JEOL 2200FS at NRL, equipped with a Thermo Noran System Six X-ray spectrometer. The SAED patterns were analyzed using the Crisp software package. Annular dark field and bright field STEM imaging and electron energy loss (EEL) spectra were obtained with the Nion UltraSTEM 100 at ORNL, equipped with a Gatan Enfina EEL spectrometer. The UltraSTEM was operated at 60 kV with a nominal probe size of 120 pm. Low-loss spectra were obtained at a dispersion of 0.05 eV ch^{-1}, with collection times of 0.5–3 ms per spectrum and integration of 30–100 spectra. Core loss spectra were recorded at 0.5 eV ch^{-1}, with collection times of 1 s, and integration of 30 spectra. The energy resolution as measured from the FWHM of the zero loss peak (ZLP) was 0.5 eV. The ZLP was subtracted from the low-loss spectra and the power law background was subtracted from the core-loss spectra using the Digital Micrograph EELS analysis package routines. The energy scale was calibrated with the C K edge 284 eV onset.

3. RESULTS AND DISCUSSION

The noble gas data are summarized in Tables 1 and 2. We include noble gas data in AC from Matsuda et al. (2010b), two Q compositions, determined by Busemann et al. (2000; "Q") and by Huss et al. (1996; "P1"), and the atmospheric values.

The ^{132}Xe concentrations, an indicator of Q abundances, of AG, AI, and AJ are 1.3×10^{-6}, 4.1×10^{-7}, and 2.1×10^{-6} cm^3 STP g^{-1}, respectively (Table 2). All fractions are further enriched in Q relative to their parent HF–HCl fraction AC (1.1×10^{-7} cm^3 STP g^{-1}). The highest enrichment is found in AJ, where Q is enriched 20 times with respect to AC. This marks the highest ^{132}Xe concentration yet observed in any Q-rich material (Figure 2(a)).

The elemental abundance patterns of these three fractions, normalized to ^{36}Ar and the average Q gas composition (Busemann et al. 2000), are shown in Figure 2(b). The noble gases in AJ are more fractionated in favor of heavy noble gases: the ^{132}Xe is 2.34 times more enriched than the average and the ^{4}He is only 28% of the average. Since He and Ne concentrations of AG and AI have been determined only as upper limits, it is difficult to discern the patterns of all five noble gases. However, the Xe in AG and AI is also enriched (1.77 times and 1.33 times, respectively) relative to the average Q composition. The Xe isotopic ratios of the three fractions are identical to those of Q within errors (Figure 3 and Table 2), and confirmed that presolar diamonds, carrying Xe-HL, is absent in these fractions.

The Ne isotopic ratios of the 600°C fraction of AJ indicate that it contains Ne of cosmogenic origin (Table 1). In a Ne three-isotope plot (Figure 4), the data points of the 600°C and 1600°C fractions lie on a straight line, indicating that the Ne in AJ is a mixture of Saratov Ne-Q and cosmogenic Ne produced by cosmic rays. The SEM-EDX analysis indicates that AJ mainly consists of carbonaceous matter with chromite grains. Since carbon is too light to produce Ne by spallation, the chromite grains most likely contain cosmogenic Ne. Cosmogenic Ne in Q, recoiled from adjacent silicates in the meteorite, is also a possibility. We checked whether a substantial amount of the cosmogenic Ne in AJ is contained in Q from the ^{21}Ne and ^{132}Xe contents (Tables 1 and 2) and abundances (Figure 1) of AC and AJ. AC and AJ produced from one gram of the Saratov meteorite contain 3.1×10^{-10} and 0.12×10^{-10} cm^3 STP of ^{21}Ne and 8.1×10^{-10} and 6.1×10^{-10} cm^3 STP of ^{132}Xe, respectively. The ^{132}Xe contents in the two fractions are comparable, indicating that the majority of the Q in AC is in AJ, while the ^{21}Ne content

Table 1
Helium, Ne, Ar, and Kr in the Saratov Fractions

	^{4}He ($\times10^{-5}$cm^3 STP g^{-1})	^{22}Ne ($\times10^{-8}$cm^3 STP g^{-1})	^{20}Ne/^{22}Ne	^{21}Ne/^{22}Ne	^{36}Ar ($\times10^{-6}$cm^3 STP g^{-1})	^{38}Ar/^{36}Ar	^{40}Ar/^{36}Ar	^{84}Kr ($\times10^{-8}$cm^3 STP g^{-1})
AG(10.1 ± 0.2 μg)								
600°C	$\leqslant$14	$\leqslant$10	...	...	13	0.1896 ± 0.0013	197.4 ± 4.0	9.7
1600°C	$\leqslant$17	$\leqslant$51	...	...	45	0.1928 ± 0.0011	18 ± 65	41
Total	$\leqslant$31	$\leqslant$61	...	...	58	0.1921 ± 0.0009	58 ± 50	51
AI (32.5 ± 0.2 μg)								
600°C	3.6	8.9	15.4 ± 4.8	0.101 ± 0.046	8.4	0.1948 ± 0.0012	241.8 ± 3.0	16
1600°C	$\leqslant$5.7	$\leqslant$14	...	...	15	0.1924 ± 0.0010	$\leqslant$2.1	13
Total	$\leqslant$9.4	$\leqslant$23	...	...	23	0.1933 ± 0.0008	...	28
AJ (109.6 ± 0.1 μg)								
600°C	2.6	5.9	5.84 ± 0.79	0.475 ± 0.093	6.0	0.1907 ± 0.0007	17.1 ± 1.6	7.1
1600°C	7.3	22	9.78 ± 0.35	0.089 ± 0.007	62	0.1873 ± 0.0006	2.5 ± 1.4	66
Total	9.9	28	8.96 ± 0.32	0.170 ± 0.020	68	0.1876 ± 0.0005	3.8 ± 1.3	73
AC (3.63 mg)								
Total	2.57	6.10	2.739 ± 0.034	0.678 ± 0.004	3.35	0.1934 ± 0.0002	9.9 ± 0.1	5.21
Saratov bulk (248.7 mg)								
Total	2.18	10.3	0.799 ± 0.004	0.859 ± 0.003	0.0677	0.2835 ± 0.0004	889.0 ± 9.3	0.0686
Q			10.05–10.70	0.0291–0.0321		0.18727 ± 0.00070		
P1						0.1875 ± 0.0010		
Air			9.800	0.029		0.1880	295.5	

Notes. The errors are 1σ. AC and Saratov bulk: Matsuda et al. (2010b); Q: Busemann et al. (2000); P1: Huss et al. (1996); Air: see Ozima & Podosek (2002) for references.

Table 2
Xenon in the Saratov Fractions

	^{132}Xe ($\times 10^{-8}$cm^3 STP g^{-1})	^{124}Xe/^{132}Xe ($\times$100)	^{126}Xe/^{132}Xe ($\times$100)	^{128}Xe/^{132}Xe ($\times$100)	^{129}Xe/^{132}Xe ($\times$100)	^{130}Xe/^{132}Xe ($\times$100)	^{131}Xe/^{132}Xe ($\times$100)	^{134}Xe/^{132}Xe ($\times$100)	^{136}Xe/^{132}Xe ($\times$100)
AG (10.1 $\pm$ 0.2 μg)									
600°C	10	0.36 $\pm$ 0.26	0.30 $\pm$ 0.21	6.58 $\pm$ 1.22	114.8 $\pm$ 8.0	15.9 $\pm$ 1.9	85.7 $\pm$ 6.8	36.5 $\pm$ 2.5	31.2 $\pm$ 1.7
1600°C	120	0.523 $\pm$ 0.088	0.29 $\pm$ 0.086	8.15 $\pm$ 0.33	107.1 $\pm$ 1.8	15.75 $\pm$ 0.51	82.83 $\pm$ 0.99	38.19 $\pm$ 1.24	33.3 $\pm$ 1.1
Total	130	0.511 $\pm$ 0.084	0.292 $\pm$ 0.081	8.03 $\pm$ 0.32	107.7 $\pm$ 1.7	15.77 $\pm$ 0.49	83.05 $\pm$ 1.05	38.06 $\pm$ 1.16	33.2 $\pm$ 1.1
AI (32.5 $\pm$ 0.2 μg)									
600°C	7.6	0.45 $\pm$ 0.14	0.49 $\pm$ 0.19	7.91 $\pm$ 0.58	112.2 $\pm$ 4.5	16.13 $\pm$ 0.73	83.8 $\pm$ 5.9	39.7 $\pm$ 1.9	34.2 $\pm$ 3.4
1600°C	33	0.449 $\pm$ 0.090	0.452 $\pm$ 0.072	8.39 $\pm$ 0.44	99.5 $\pm$ 2.3	15.84 $\pm$ 0.37	82.3 $\pm$ 1.8	37.43 $\pm$ 0.92	30.88 $\pm$ 0.83
Total	41	0.450 $\pm$ 0.077	0.459 $\pm$ 0.068	8.30 $\pm$ 0.37	101.9 $\pm$2.1	15.89 $\pm$ 0.33	82.6 $\pm$ 1.9	37.86 $\pm$ 0.82	31.51 $\pm$ 0.92
AJ (109.6 $\pm$ 0.1 μg)									
1600°C	10	0.497 $\pm$ 0.085	0.33 $\pm$ 0.14	7.71 $\pm$ 0.47	113.7 $\pm$ 3.1	16.16 $\pm$ 0.49	81.9 $\pm$ 2.1	37.85 $\pm$ 1.06	32.11 $\pm$ 0.68
1600°C	200	0.479 $\pm$ 0.024	0.425 $\pm$ 0.033	8.38 $\pm$ 0.12	104.59 $\pm$ 0.51	15.96 $\pm$ 0.14	81.70 $\pm$ 0.65	37.55 $\pm$ 0.36	31.92 $\pm$ 0.31
Total	210	0.480 $\pm$ 0.024	0.421 $\pm$ 0.032	8.34 $\pm$ 0.11	105.02 $\pm$ 0.79	15.97 $\pm$ 0.13	81.71 $\pm$ 0.63	37.57 $\pm$ 0.35	31.93 $\pm$ 0.30
AC (3.63 mg)									
Total	10.6	0.47 $\pm$ 0.01	0.42 $\pm$ 0.01	8.23 $\pm$ 0.03	105.10 $\pm$ 0.21	16.13 $\pm$ 0.09	82.25 $\pm$ 0.14	38.01 $\pm$ 0.11	31.59 $\pm$ 0.09
Saratov bulk (248.7 mg)									
Total	0.168	0.45 $\pm$ 0.01	0.41 $\pm$ 0.01	8.35 $\pm$ 0.05	124.4 $\pm$ 0.60	16.20 $\pm$ 0.07	82.01 $\pm$ 0.20	38.10 $\pm$ 0.24	32.04 $\pm$ 0.21
Q		0.455 $\pm$ 0.002	0.4057 $\pm$ 0.0018	8.22 $\pm$ 0.02	104.2 $\pm$ 0.2	16.19 $\pm$ 0.03	81.85 $\pm$ 0.09	37.80 $\pm$ 0.11	31.64 $\pm$ 0.08
P1		0.467 $\pm$ 0.006	0.414 $\pm$ 0.005	8.30 $\pm$ 0.03	104.0 $\pm$ 0.2	16.30 $\pm$ 0.04	82.12 $\pm$ 0.12	37.79 $\pm$ 0.11	31.65 $\pm$ 0.10
Air		0.3537 $\pm$ 0.0011	0.3300 $\pm$ 0.0017	7.136 $\pm$ 0.009	98.32 $\pm$ 0.12	15.136 $\pm$ 0.012	78.90 $\pm$ 0.11	38.79 $\pm$ 0.06	32.94 $\pm$ 0.04

Notes. The errors are 1σ. AC and Saratov bulk: Matsuda et al. (2010b); Q: Busemann et al. (2000); P1: Huss et al. (1996); Air: see Ozima & Podosek (2002) for references.

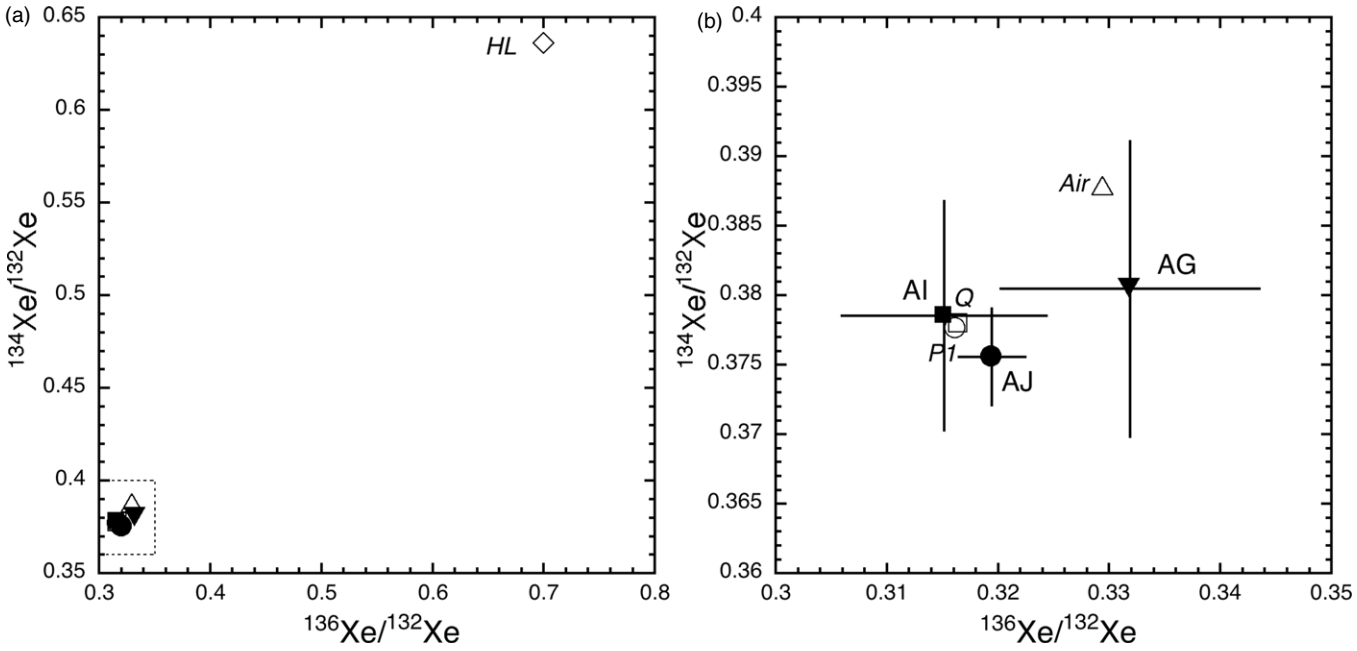

Figure 3. Total $^{134}Xe/^{132}Xe$ ratios of AG, AI, and AJ are plotted against the total $^{136}Xe/^{132}Xe$ ratios. (a) The Xe in all fractions cluster around Q (=P1), indicating that there is no Xe-HL in these fractions. (b) The dotted area in (a) is enlarged.

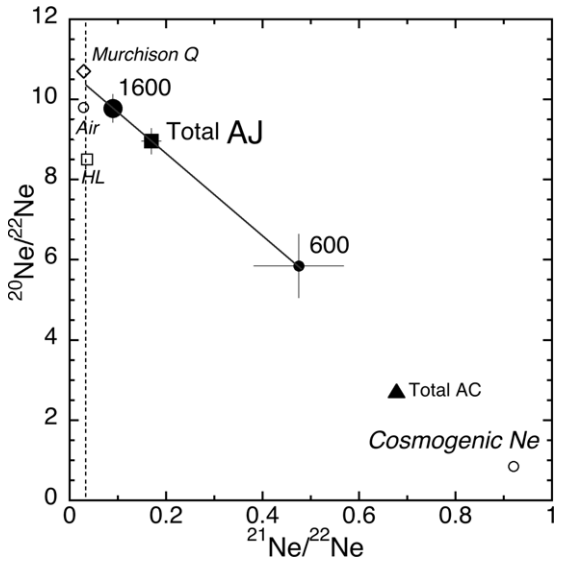

Figure 4. Ne isotopic composition of AJ is shown in a three-isotope plot. The total Ne of AC, Murchison Ne-Q, Ne-HL (in presolar diamond), and cosmogenic Ne are also shown. The Ne in AC consists mainly of cosmogenic Ne. The fraction of cosmogenic Ne in AJ is much less than that in AC. The solid line connects the two temperature fractions and indicates that the Ne in AJ is mixture of Saratov Ne-Q and cosmogenic Ne. We extrapolated the line and took the $^{20}Ne/^{22}Ne$ ratio at $^{21}Ne/^{22}Ne = 0.0320$ as Satatov Ne-Q.

of AJ is ∼4% of AC. These numbers indicate that Q is not the major carrier of cosmogenic Ne.

To determine the $^{20}Ne/^{22}Ne$ ratio of Saratov Ne-Q from a Ne three-isotope plot, we extrapolated the line connecting the points for the 600°C and 1600°C fractions of AJ to $^{21}Ne/^{22}Ne = 0.0320$ (Figure 4). This is the ratio Matsuda et al. (2010b) determined as the $^{21}Ne/^{22}Ne$ ratio of Saratov Ne-Q. Using their $^{21}Ne/^{22}Ne$ ratio, the $^{20}Ne/^{22}Ne$ of Saratov Ne-Q was determined to be 10.36 ± 0.43. This is consistent with the previous result ($^{20}Ne/^{22}Ne = 9.84 \pm 0.18$) obtained by Matsuda et al. (2010b), but with a larger error. It has been known that $^{20}Ne/^{22}Ne$ ratios of Q-rich fractions from various meteorites fall into two groups (Huss et al. 1996; Busemann et al. 2000): one with $^{20}Ne/^{22}Ne$ around 10.1 as observed in Julesburg (L3.6), Abee (EH4), Cold Bokkeveld (CM2), and Lancé (CO3.5), and the other one with $^{20}Ne/^{22}Ne$ round 10.7, as seen in Chainpur (LL3.4), Grosnaja (CV3), and Dimmitt (H3.7). The uncertainty in the $^{20}Ne/^{22}Ne$ value of Saratov Ne-Q makes it consistent with both groups, although the result by Matsuda et al. (2010b) supports that Saratov Ne-Q belongs to the first group.

The TEM studies reveal that two materials are present in the Q-rich AJ and AI separates: carbon and chromite (Figure 5(a)). The carbon appears disordered and porous in HRTEM images (Figure 5(b)). The identity of the chromite nanoparticles was confirmed with EDS (not shown) and analysis of the discrete spots that appear in some of the SAED patterns (Figure 5(c)). We discount the possibility that the chromite grains contain significant Q gases: chromite grains survive $Cr_2O_7^{2-}$ treatment that destroys Q (Tang & Anders 1988). No nanodiamond, graphite, and SiC were observed, which is consistent with the previous noble gas study by Huss & Lewis (1995) that showed the abundances of these noble gas carriers decrease with increasing petrologic type. In addition to the chromite diffraction spots, two rings are present in the SAED patterns from both AI (not shown) and AJ samples (Figure 5(c)). The rings (Figure 5(c), labels 1 and 2) correspond to 0.213 nm and 0.127 nm d-spacings, respectively, which index to a random distribution of (1 0 0) and (1 1 0) nanometer scale graphene domains. The lack of rings with (*hkl*) indices with $l \neq 0$ indicates that the graphene domains are randomly arranged without long-range graphitic order. In lower magnification STEM images, thinner regions of the carbon can resemble carbon onions (Figure 5(d), white square). However, in high-resolution STEM imaging of these areas at 60 kV (Figure 5(e)) the planar carbon ring structure of graphene domains can be observed. The BF and annular dark-field STEM images (Figure 5(f)) show local variation in graphene domain size, flatness, edge termination, and packing. The edges of some domains appear to be curled (Figure 5(e)), connecting back on themselves

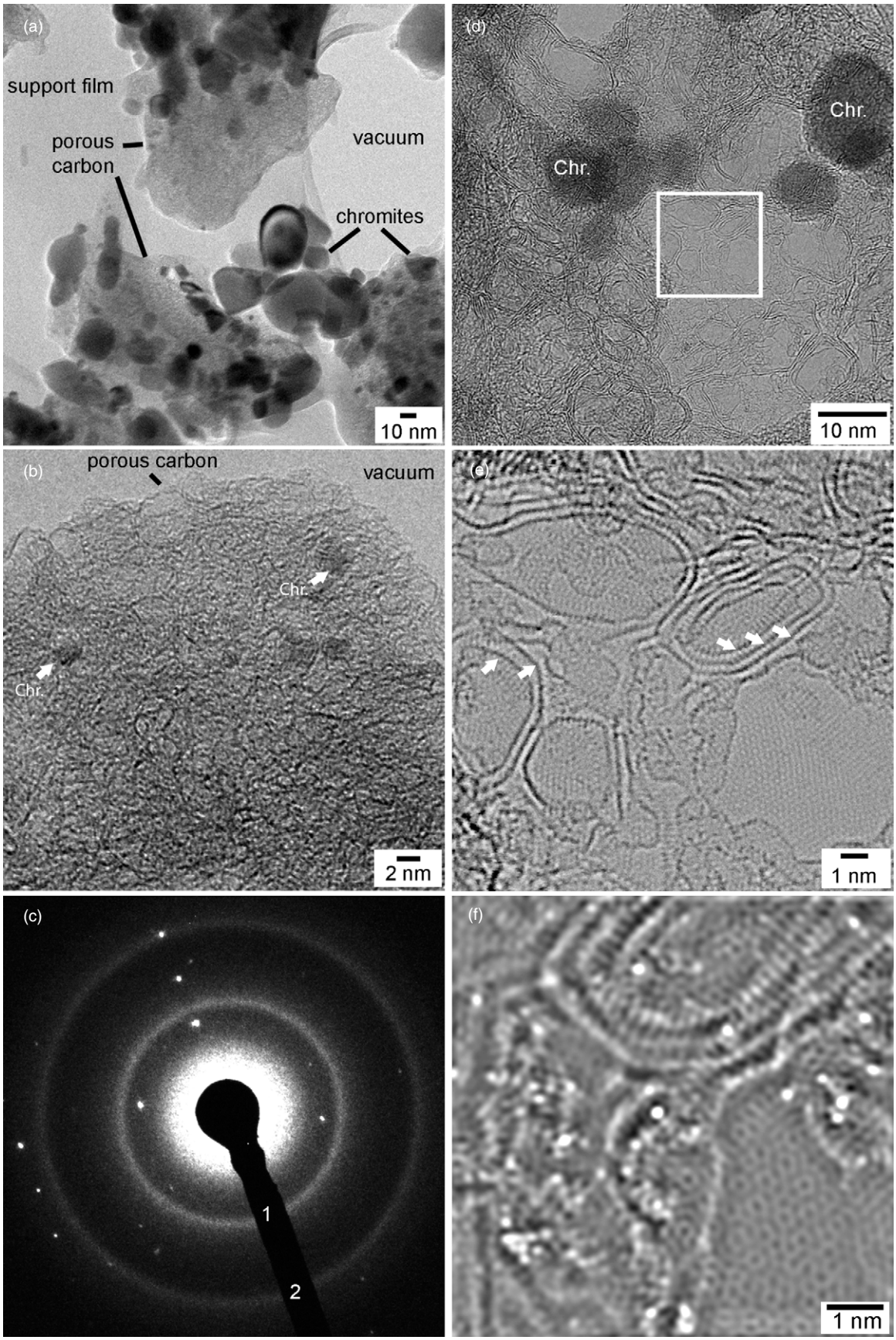

Figure 5. (a) Bright-field TEM image of AI. (b) High-resolution TEM image of AJ. The label Chr. refers to chromite nanoparticles. (c) Selected area electron diffraction pattern of AJ. The labels 1 and 2 refer to the (1 0 0) and (1 1 0) spacings of graphene. The lack of rings corresponding to $\langle hkl \rangle$ with $l \neq 0$ indicates that there is no long-range graphitic order. (d) Bright-field STEM image of AI. The white box indicates the field of view of subpanel (e). (e) Higher magnification bright-field STEM image of AI. The white arrows indicate curled edges of carbon platelets. (f) FFT-filtered annular dark-field image of AI of a sub-region of the area shown in (e). The bottom right corner of the image shows a single-sheet region in which the ring structure is resolved. Individual white spots are impurity atoms, including O, S, and Cr.

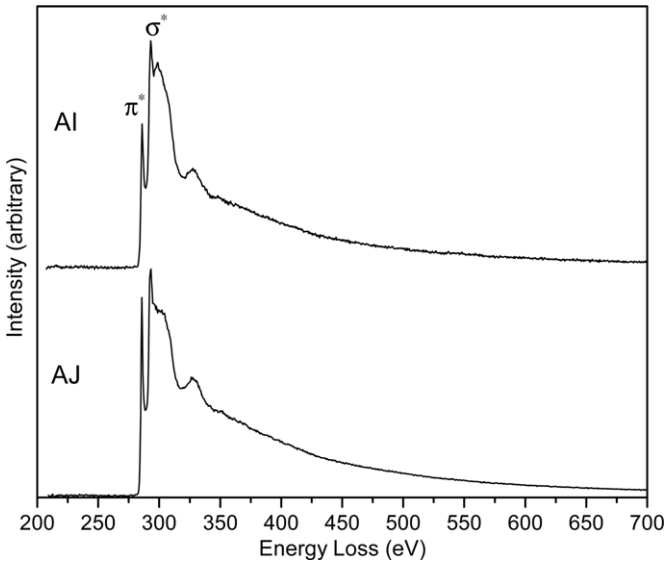

Figure 6. Electron energy loss spectra from AI and AJ. The C K edge spectra for both samples are indicative of sp^2-bonded carbon with short-range graphitic order. Only C was detected in the carbonaceous materials; Ar (245 eV), Cr (574 eV), O (532 eV), and Xe (672 eV) were not observed.

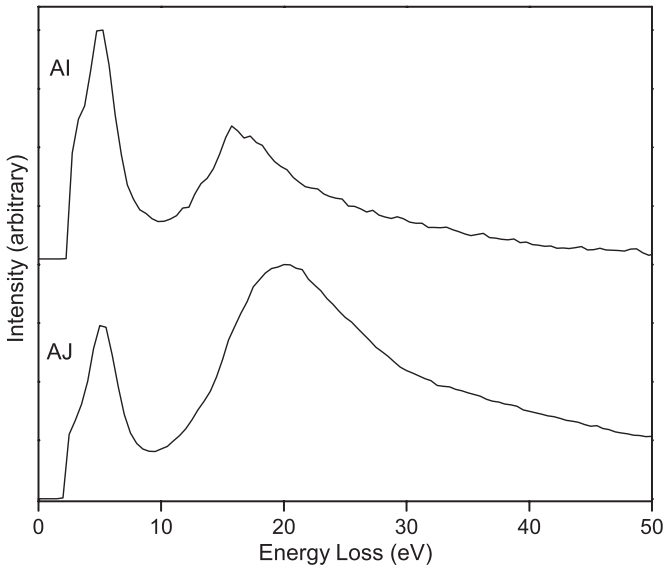

Figure 7. Low-loss electron energy loss spectra from AI and AJ. The zero loss peak was subtracted from both spectra. The two remaining peaks correspond to the surface (π) and bulk ($\pi-\sigma$) plasmons, respectively. The Ar M (12 eV) and He K (21.2 eV) edges were not detected.

or adjacent domains. Tubular edge termination is calculated to be an energetically favorable structure for graphene nanoribbons (Ivanovskaya et al. 2011) that are not H-terminated.

The C K edge EEL spectra of the carbonaceous portions of AI and AJ confirm (Figure 6) that both samples are predominately sp^2 bonded with short-range, graphite-like order (Egerton 2011). The Ar $L_{2,3}$ edge, if detectable, would appear at 245 eV, but was not observed in either sample. Similarly, the Xe $M_{4,5}$, which occurs at 645 eV, was not observed. The O K edge (532 eV) was also absent from the spectra of the carbonaceous material. The low-loss spectra (Figure 7) show two peaks, one at 5 eV and one at 16–20 eV, corresponding to the surface (π) and bulk ($\pi-\sigma$) plasmons, respectively. The position of the bulk plasmon was observed to shift to higher energy as a function of the number of stacked graphene platelets; however it is well below the bulk

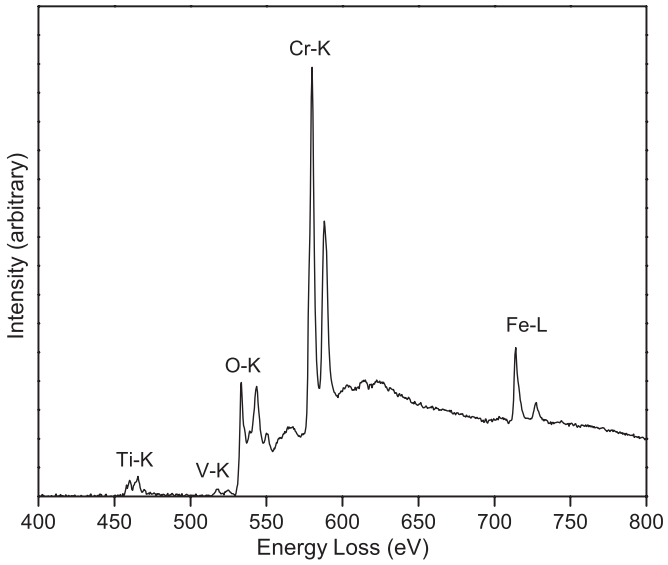

Figure 8. Electron energy loss spectrum from a chromite grain. The chromite contains minor Ti and V in addition to Cr, Fe, and O.

plasmon value of graphite at 27 eV. He and Ar have adsorption edges at 21.2 and 12 eV, respectively; however, neither of these was observed. An example core loss spectrum (Figure 8) from a chromite was also obtained. This grain shows Ti and V, in addition to Cr, Fe, and O.

The gas permeability of graphene membranes is extremely low, even for gasses as light as He. Thus, it is plausible that Q gases could be stored in pockets between nanoscale graphene membranes or in curled domain edges for Gyr timescales. Porous carbons in general have high surface areas and porosities (e.g., Lu et al. 2005) that are conducive to gas storage, which makes them an attractive candidate for Q. The gas storage properties, such as capacity for different gases and temperature of release, depend in detail on the size, shape, and spatial distribution of pores that act as trapping sites. The fact that the noble gases in Q are heavily enriched in heavy noble gases relative to solar composition strongly suggests that adsorption in low temperatures took place. However, the retention in Q of noble gases over a ~4.5 Gyr timeframe that includes thermal metamorphism on the Saratov parent body (>650°C), is incompatible with simple surface adsorption. More robust incorporation by physical entrapment, e.g., active capture (Hohenberg et al. 2002), ion implantation, or chemical bonding of ionized gas atoms to the carbon network (Matsuda & Yoshida 2001; Marrocchi et al. 2011) is required.

Although the Xe concentration in AJ is the highest ever obtained in Q-rich materials, the Xe/C atomic ratio of AJ is still 6.2×10^{-9}. Assuming a density of the porous carbon of ~1.5 g cm^{-3}, and a homogenous distribution of Xe, there are 10^4 C and 10^{-5} Xe atoms nm^{-2} where the carbon is 100 nm thick (regions examined with SAED and BF TEM, low magnification STEM). In the 1–10 nm thick areas examined with high-resolution STEM, there are 10^2–10^3 C atoms and 10^{-7}–10^{-6} Xe atoms nm^{-2}. The total areas observed in the lower resolution modes were $>10^7$ nm^2 for each sample, which should contain 100 Xe atoms on average. No crystalline phases of carbon were observed in these areas, only local variation in the structure of nanoscale graphene domains that make up the porous carbon. Thus, the simplest conclusion is that the Q carrier is one or more of the local arrangements of the graphene

domains. However, we have not yet detected Q gases in situ to associate them definitively with a specific atomic microstructure of the C, and we cannot completely rule out the possibility that there is a distinct crystalline carrier phase that is both rare (<1% of total carbon) and small (<5 nm) enough to escape detection with SAED, HRTEM, and STEM imaging. In principle, the location of the Xe in the carbon, whether it is held in a particular variant of graphene or in a distinct, yet to be detected phase, can be identified with atomic-resolution annular DF STEM imaging. However, the area imaged in our initial aberration-corrected STEM study (10^4 nm^2) must be increased by $>10^3$ in order to observe the Xe atoms, assuming a uniform dispersion. Other noble gas species may also be imaged directly, but the image intensity depends linearly on thickness and on atomic number, Z, to the power of 1.64. Thus, Xe, Kr, Ar, and possibly Ne are much more likely to be identified in a DF STEM image than He.

In summary, the long elusivity of Q may simply reflect that it is indistinguishable in structure and chemistry, other than in the retained noble gas content, from the 99% of other meteoritc porous carbon. The release of Q gases may simply resulted from the structural rearrangement of the carbon phase (Matsuda et al. 2010a). Alternatively, Q itself may take the form of a distinct, nanometer scale minor (<1%) phase, yet to be detected. Further concentration of Q and automated image processing of atomic-resolution DF STEM images to cover larger areas of carbon should further clarify the Q phase identification.

This work has been supported by the McDonnell Center for the Space Sciences (S.A.), the DOE Office of Basic Energy Sciences, Materials Sciences and Engineering Division (M.F.C.), and NASA grants NNH09AL201 (R.M.S.) and NNX13A48G (S.A.). We thank the two anonymous reviewers for their critical comments.

REFERENCES

Amari, S., Anders, E., Virag, A., & Zinner, E. 1990, Natur, 345, 238
Busemann, H., Baur, H., & Wieler, R. 2000, M&PS, 35, 949
Clayton, D. D. 1968, Principles of Stellar Evolution and Nucleosynthesis (New York: McGraw-Hill)
Egerton, R. 2011, Electron Energy-Loss Spectroscopy in the Electron Microscope (3rd ed.; New York: Springer)
Heber, V. S., Wieler, R., Baur, H., et al. 2009, GeCoA, 73, 7414
Hohenberg, C. M., Thonnard, N., & Meshik, A. 2002, M&PS, 37, 257
Huss, G. R., & Lewis, R. S. 1995, GeCoA, 59, 115
Huss, G. R., Lewis, R. S., & Hemkin, S. 1996, GeCoA, 60, 3311
Ivanovskaya, V. V., Zobelli, A., Wagner, P., et al. 2011, PhRvL, 107, 065502
Lewis, R. S., Srinivasan, B., & Anders, E. 1975, Sci, 190, 1251
Lewis, R. S., Tang, M., Wacker, J. F., Anders, E., & Steel, E. 1987, Natur, 326, 160
Lodders, K., & Fegley, B., Jr. 1998, The Planetary Scientist's Companion (New York: Oxford Univ. Press)
Lu, A.-H., Li, W.-C., Muratova, N., Spliethoff, B., & Schüth, F. 2005, Chem. Commun., 2005, 5184
Mahaffy, P. R., Donahue, T. M., Atreya, S. K., Owen, T. C., & Niemann, H. B. 1998, SSRv, 84, 251
Marrocchi, Y., Marty, B., Reinhardt, P., & Robert, F. 2011, GeCoA, 75, 6255
Matsuda, J., Morishita, K., Tsukamoto, H., et al. 2010a, GeCoA, 74, 5398
Matsuda, J., Tsukamoto, H., Miyakawa, C., & Amari, S. 2010b, M&PS, 45, 361
Matsuda, J., & Yoshida, T. 2001, M&PS, 36, A127
Moniot, K. M. 1980, GeCoA, 44, 253
Ott, U., Mack, R., & Chang, S. 1981, GeCoA, 45, 1751
Ozima, M., & Podosek, F. A. 2002, Noble Gas Geochemistry (2nd ed.; Cambridge: Cambridge Univ. Press)
Reynolds, J. H., Frick, U., Neil, J. M., & Phinney, D. L. 1978, GeCoA, 42, 1775
Tang, M., & Anders, E. 1988, GeCoA, 52, 1235
Verchovsky, A. B., Sephton, M. A., Wright, I. P., & Pillinger, C. T. 2002, E&PSL, 199, 243
Wacker, J. F. 1989, GeCoA, 53, 1421
Wacker, J. F., Zadnik, M. G., & Anders, E. 1985, GeCoA, 49, 1035
Wieler, R., Anders, E., Baur, H., Lewis, R. S., & Signer, P. 1991, GeCoA, 55, 1709
Wieler, R., Anders, E., Baur, H., Lewis, R. S., & Signer, P. 1992, GeCoA, 56, 2907
Zadnik, M. G., Wacker, J. F., & Lewis, R. S. 1985, GeCoA, 49, 1049